Hindawi
Journal of Spectroscopy
Volume 2018, Article ID 1074734, 8 pages
https://doi.org/10.1155/2018/1074734

Research Article

$\Delta E/\Delta E$ Measurements of Energetic Ions Using CVD Diamond Detectors

Ahmed Alghamdi, Lawrence Heilbronn, Luis A. Castellanos, and Eric Lukosi

Department of Nuclear Engineering, University of Tennessee, Knoxville, TN 37922, USA

Correspondence should be addressed to Ahmed Alghamdi; aalgham2@vols.utk.edu

Received 15 January 2018; Revised 30 March 2018; Accepted 10 May 2018; Published 20 June 2018

Academic Editor: Eugen Culea

Experimental and computational results of a $\Delta E/\Delta E$ diamond detection system are presented. The $\Delta E/\Delta E$ detection system was evaluated using energetic proton and iron beams striking thick polyethylene targets at the NASA Space Radiation Laboratory (NSRL) at Brookhaven National Laboratory (BNL). The measured data for diamond sensor A show good agreement with the Geant4 simulation. In addition, simulations have demonstrated the ability to identify hydrogen isotopes using a diamond detection system.

1. Introduction

Diamond is an attractive material because of its many electrical, chemical, and mechanical characteristics [1–4]. Its consistent application in radiation sensing occurred after synthetic chemical vapor deposition (CVD) growth of diamond was demonstrated to produce consistent and suitable properties [5, 6]. Since then, diamond detectors have been explored for use in extreme environments [7–11], microdosimetry [12, 13], and thermal [10, 14, 15] and fast neutron sensing [10, 16–20], including deuterium-deuterium (DD) and deuterium-tritium (DT) fusion plasma diagnostics [21, 22]. One extreme environment under consideration for diamond detectors is high-rate particle tracking sensors at the LHC [7, 23–26]. Its large displacement energy (43 eV) results in a high radiation hardness [27], and its 5.5 eV band gap enables operation at room temperature without the need of heat sinks [1]. Its high saturation velocity (mobility) of both holes and electrons yields an excellent timing resolution [5, 28, 29]. These essential attributes make diamond sensors a potential candidate for current silicon detector replacement technology in high-energy physics tracking experiments [30–32].

In this paper, we present results on a $\Delta E/\Delta E$ diamond detection system for secondary particles produced by proton and iron energetic beams striking thick polyethylene targets. Geant4 simulations are used to benchmark and understand experimental observations, with a focus on particle identification using time of flight (ToF) [25, 33–36].

2. Experimental Setup

A schematic view of the $\Delta E/\Delta E$ diamond detection system is shown in Figure 1. Two parallel electronic-grade single-crystal CVD diamonds (diamonds A and B) were separated by 2 cm, where the top sensor was diamond A. Both diamond detectors are $4\,\text{mm} \times 4\,\text{mm} \times 0.45\,\text{mm}$ in dimension. Each detector was cleaned using aqua regia followed by chromium etchant. After that, sensors were metalized with an Au/Cr contact scheme via RF magnetron sputtering. Following metallization, each detector was annealed in 10 mTorr of argon gas for 20 minutes. Finally, each diamond detector was mounted onto a printed circuit board (PCB), both mounted within an aluminum enclosure containing two CR-110 charge-sensitive preamplifiers.

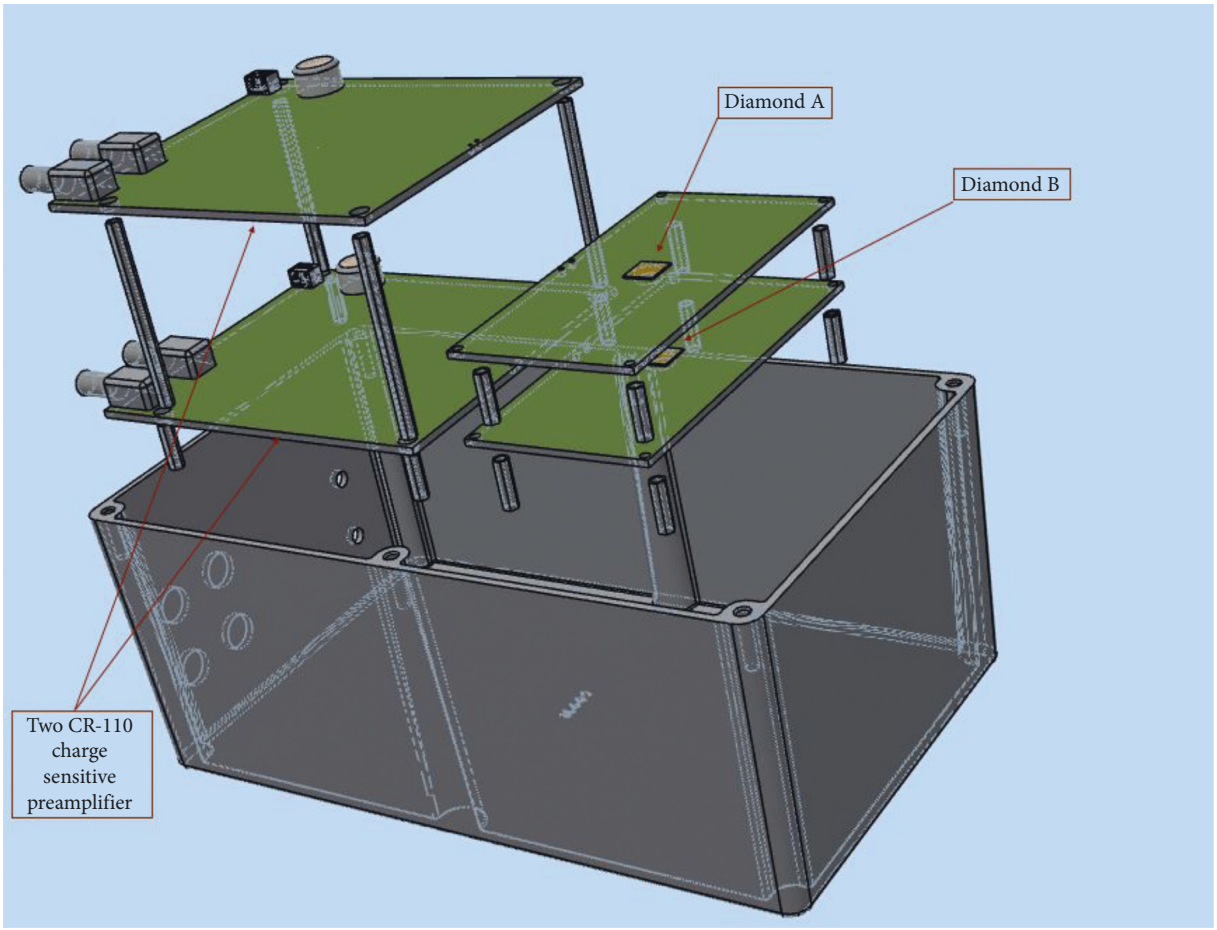

Figure 1: Layout of the sensors inside the aluminum enclosure.

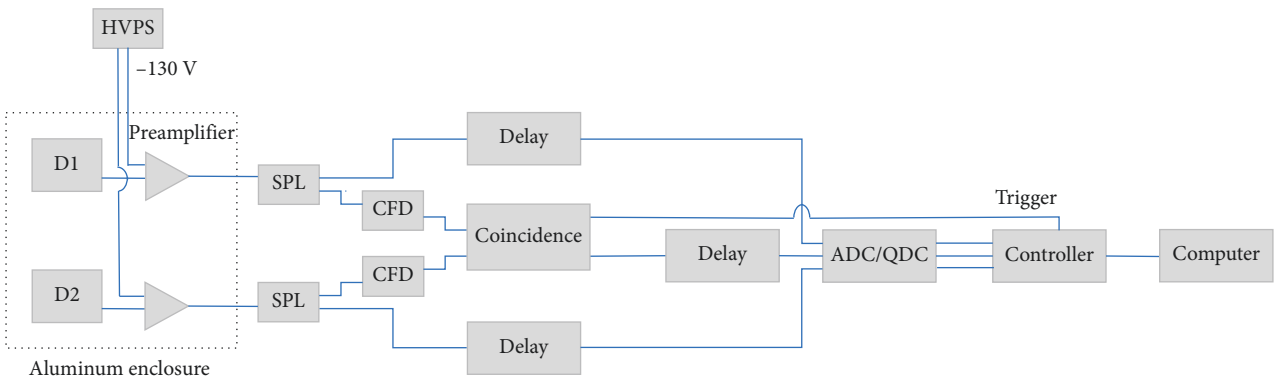

Figure 2: A schematic of the signal chain of the $\Delta E/\Delta E$ detection system.

The analog signal from each detector, after preamplification, was divided into two pulses using an NSRL splitter. The first pulse was delayed before being fed into the digital acquisition system. The other pulse from each detector was fed into a constant fraction discriminator (CFD), and each output was fed into a fast-coincident module to trigger true minimum ionizing particle (MIP) events for collection by the digital acquisition system. Data were analyzed online through a modified acquisition framework [36]. A schematic diagram of the electronics is shown in Figure 2.

The experiment was conducted at the NASA Space Radiation Laboratory (NSRL) at Brookhaven National Laboratory (BNL) in December 2016. The experimental arrangement is shown in Figure 3. Two thick polyethylene targets were situated along the beamline. The upstream

target had a thickness of 20, 40, or 60 g/cm^2, while the thickness of the downstream target was 60 g/cm^2. These targets were separated by 3.5 meters down the beam. The high-energy beams striking the target were 1 cm in diameter, consisting of either protons (400 MeV, 800 MeV, and 2.5 GeV) or iron (400 AMeV). Two detector positions were selected based on beam species and energy. In the first position, the detection system was located along the beam axis (0°) and behind the backstream target for 800 MeV and 2.5 GeV protons since they penetrate through both targets. In the second position, the detection system was placed 45° off the beam axis to measure scattered protons/iron and secondary particles at 400 AMeV.

3. Geant4 Simulations

The simulated interaction of the proton and iron beams with polyethylene targets and production of secondary ions were implemented using Geant4 [35]. The Bertini intranuclear cascade with a high precision neutron (lower than 20 MeV) model was used to simulate energetic ion interaction for all projectiles [37]. The NSRL room geometry was modeled including targets, concrete floor, walls [38], and the $\Delta E/\Delta E$ diamond detection system. The beamline rail system and other equipment within the room were not included in the simulation. The incident beam (or particle) was located 70 cm upstream from the front target and was simulated as a monoenergetic and monodirectional point source. The simulation results were normalized and plotted using the same bins width of the measured response of the diamond detection system. The CFD threshold was set to prevent low-energy false coincidences, which was accounted for in the Geant4 simulation to provide adequate agreement with experimental spectra.

4. Results

The simulated and experimental energy spectra for the 800 MeV proton beam are shown in Figure 4. The response of diamond sensor A agrees well with computational results. However, diamond sensor B exhibits significantly less pulse height for the primary peak and an overall different shape, where simulations indicate that the signal in the two detectors should be nearly identical. The detection system operates in coincidence between diamond detectors A and B, and both diamonds recorded the same number of events. We further investigated the observed difference in the spectra by changing the orientation of the detection system with respect to the beam vector, and the same result was observed, indicating that the observed differences are not due to secondary particle generation in the front diamond detector striking the back diamond detector. We hypothesize that the observed differences are due to poor metal contact-diamond interface properties along with natural differences in gain between the two preamplifiers.

The response of diamond detector A, compared with the simulated results with different upstream target thicknesses, is provided in Figure 5. Geant4 simulations observed proton, pion, positron, and electron interactions for all simulations. The pions, positrons, and electrons manifest themselves in the lowest energy region of the energy spectrum (on the order of tens of keV), while the protons comprise the primary peak(s), which is responsible for >90% of the observed counts (Figure 6). The measured spectra at 800 MeV show a few peaks due to the different thicknesses of the upstream target, which is due to the higher rates of energy deposition from slower moving ions exiting the thicker targets [39]. For the 2.5 GeV proton beam, simulations indicate that the energy deposition is almost constant for all thicknesses since the secondary particles are located on the minimum stopping power region in the proton stopping power graph [40]. Nevertheless, the measured spectra exhibit two peaks versus one peak in the simulation (Figure 5(a)), which is likely a consequence of the simple geometry simulated and slight variation in the location of a diamond sensor.

For 400 MeV proton beam, the detection system was located at position 2, resulting in significantly lower observed counts, requiring deactivation of the coincidence mode. The simulations indicate that fast neutron-induced alpha particles and scattered carbon nuclei are created, contributing mainly in the lowest energy region of the spectrum, as shown in Figure 6(c). However, the small fast neutron cross section with carbon resulted in a minute contribution to the overall observed response [41]. In addition, protons, pions, positrons, and electrons were observed from proton interactions with the polyethylene target (Figure 5(f)). The number of detected pions and electrons is higher for the 400 MeV proton beam than for the other proton beams because it deposited a higher energy within the polyethylene target and consequently liberated more secondary particles than 800 MeV and 2.5 GeV proton projectiles.

From the Geant4 simulation of the 400 AMeV iron beam on the 20 g/cm^2 upstream target, isotopes of hydrogen were identified using stopping power (dE/dx) in detector A and kinetic energy of the particle, as shown in Figure 7. Kinetic energy was reconstructed using relativistic kinematics and the simulated ToF between the two sensors [42]. Comparing computational stopping power of proton in the diamond detector and NIST graphite target shows that the general slope shape of the stopping power curve is achieved [40]. However, the diamond detector shows higher stopping power for energies greater than 100 MeV due its higher density.

5. Conclusion

The measured spectra for diamond sensor A exhibits good agreement with Geant4 simulations for proton beams. The diamond detector B exhibited poor response, perhaps due to poor electrical connections and/or front-end electronics. A wide energy range of produced proton particles made it impractical to distinguish between different ions using only $\Delta E1$. However, increasing the separation distance between the two diamonds with appropriate fast electronics could

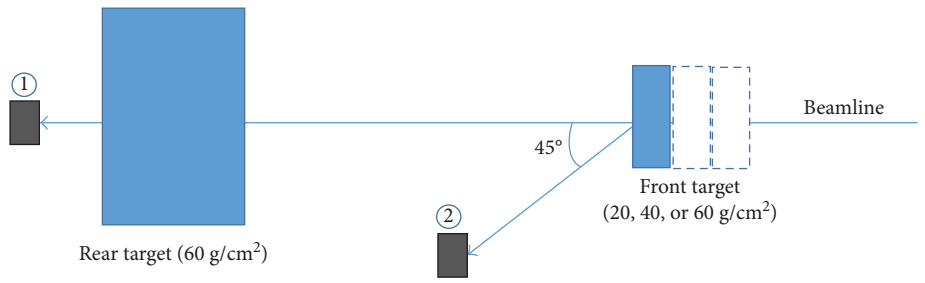

Figure 3: $\Delta E/\Delta E$ detection system arrangements.

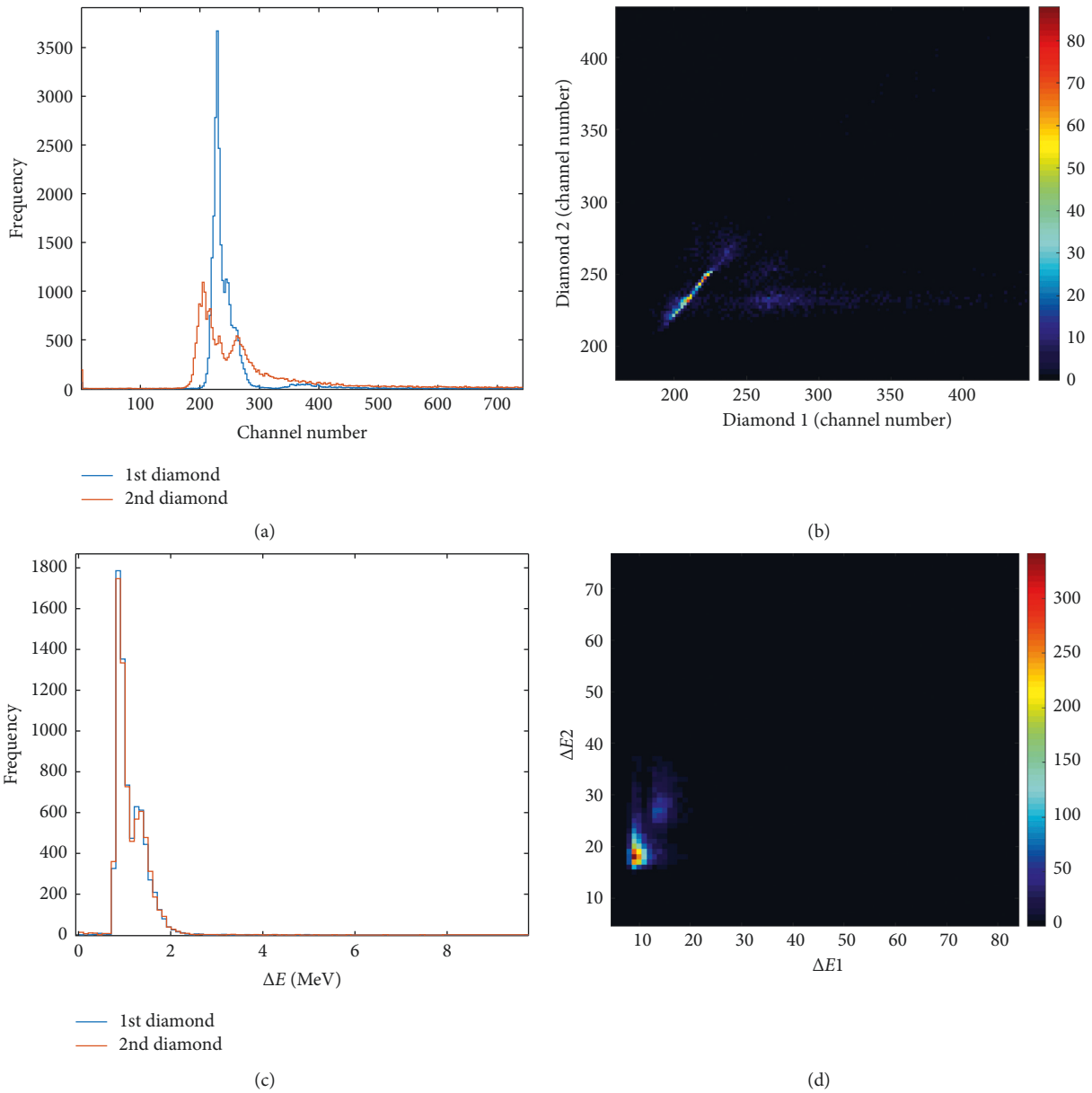

Figure 4: 800 MeV proton beam: (a) measured spectra of each diamond, (b) experimental energy depositions in both detectors, (c) Geant4 simulation spectra in the two diamond sensors, and (d) simulated $\Delta E1$ versus $\Delta E2$.

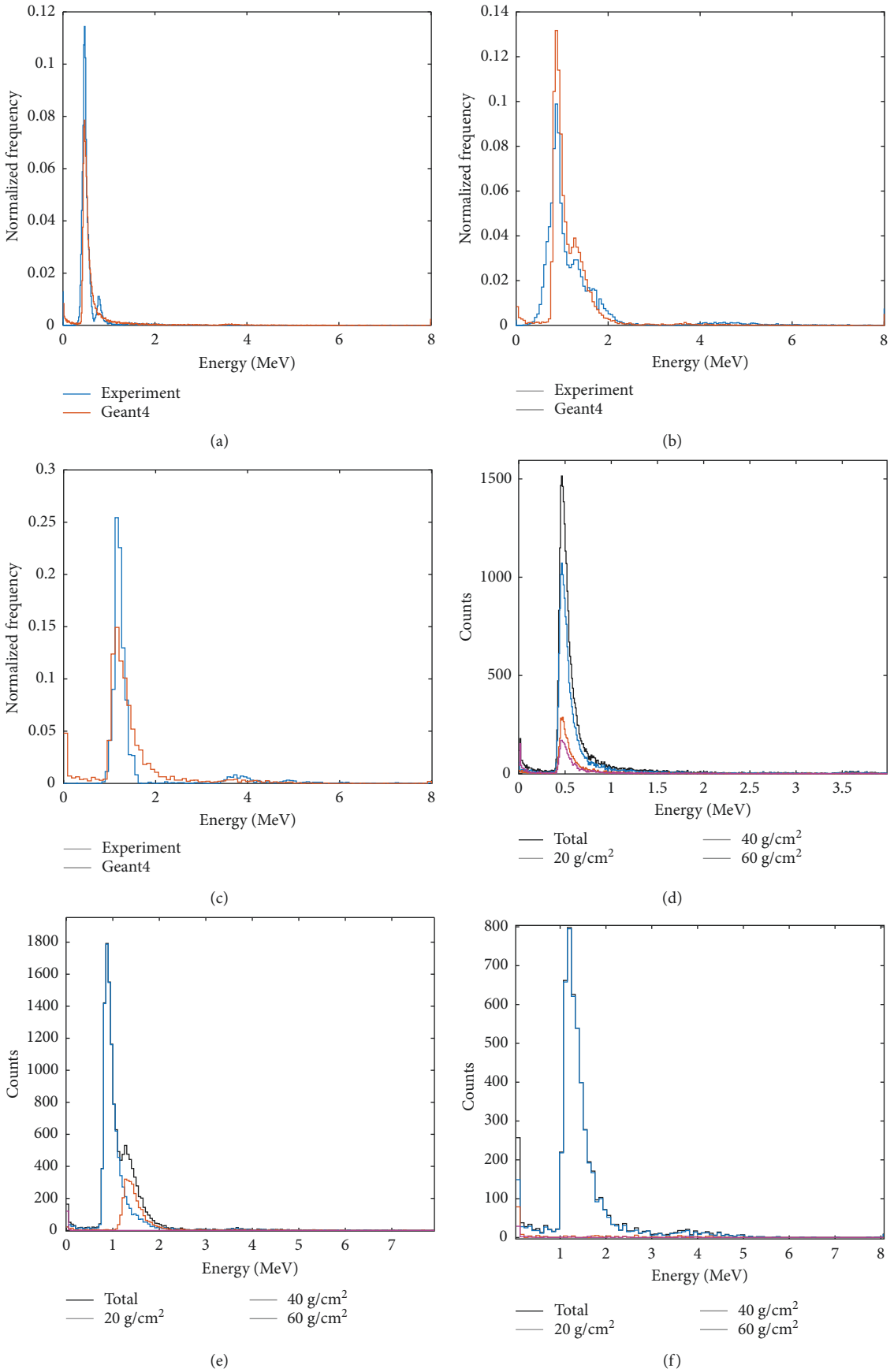

Figure 5: Experimental versus simulation spectra for (a) 2.5 GeV, (b) 800 MeV, and (c) 400 MeV proton beams, respectively. Simulated spectra for different upstream target thicknesses: (d) 2.5 GeV, (e) 800 MeV, and (f) 400 MeV.

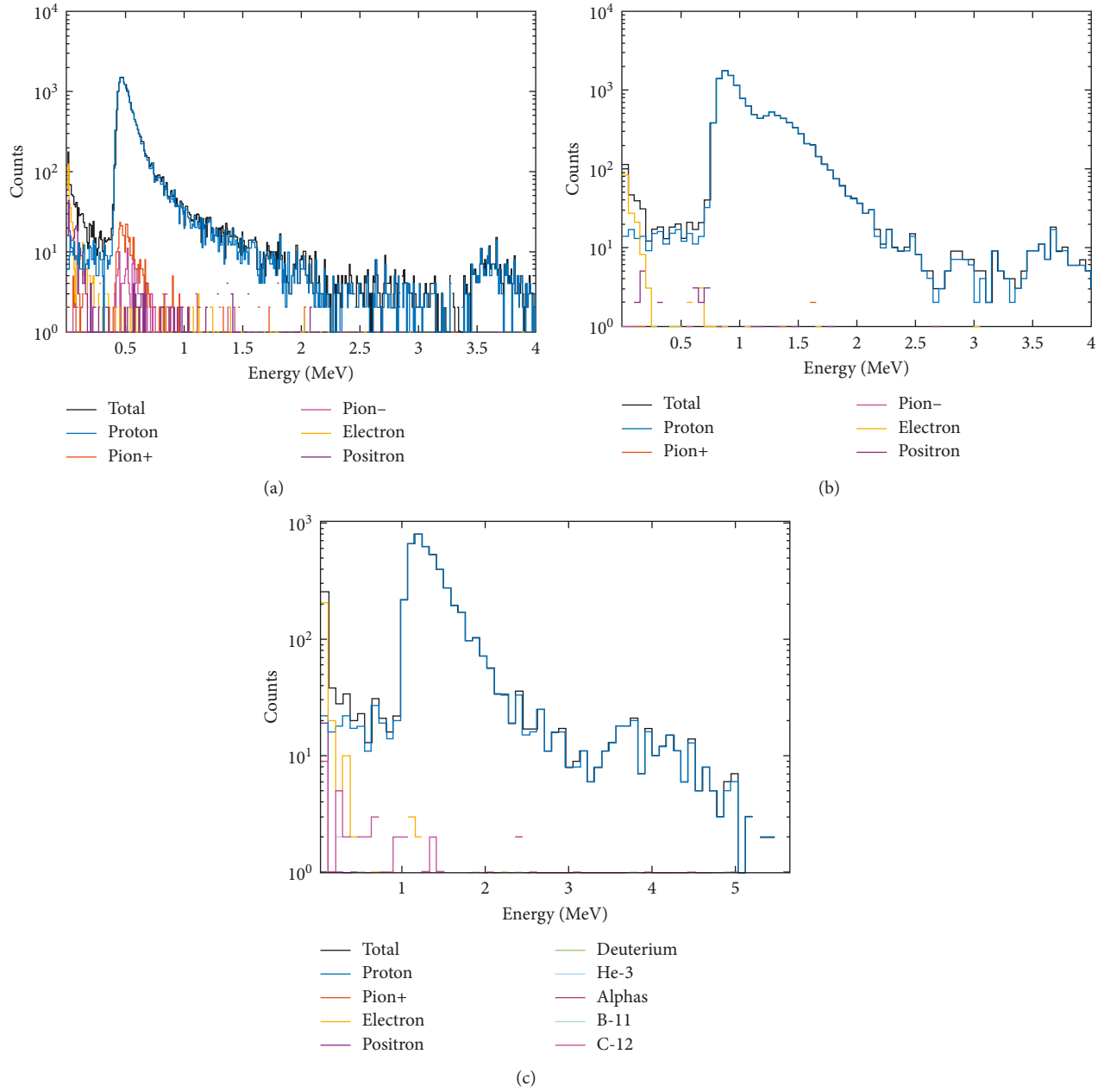

Figure 6: Interacted particles with the diamond sensor A for proton beams: (a) 2.5 GeV, (b) 800 MeV, and (c) 400 MeV.

lead to particle discrimination between energetic light ions using ToF.

Data Availability

The data used to support the findings of this study are available from the corresponding author upon request.

Disclosure

Part of this research was conducted in the Micro-Processing Research Facility, a core facility of the University of Tennessee.

Conflicts of Interest

The authors declare that there are no conflicts of interest regarding the publication of this paper.

Acknowledgments

The authors would like to express their gratitude to Mike Sivertz and Adam Rusek of the NASA Space Radiation Laboratory at Brookhaven National Laboratory for their assistance. Also, the first author would like to thank the King Abdulaziz City for Science and Technology (KACST) for sponsoring his Ph.D. studies at the University of Tennessee.

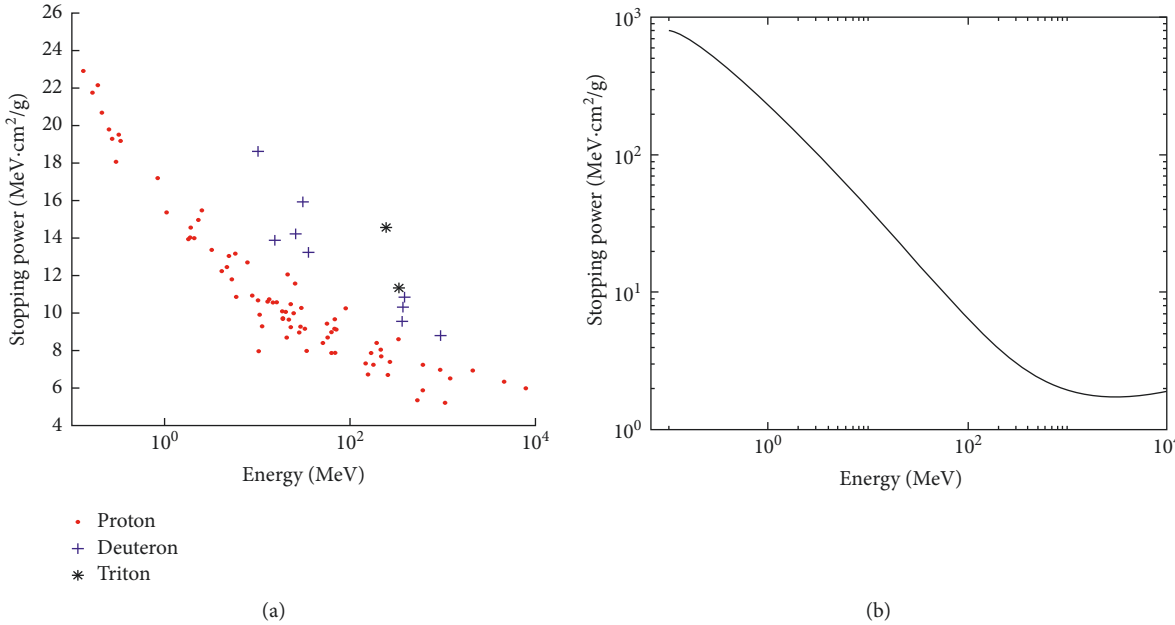

FIGURE 7: (a) Kinetic energy versus first diamond energy stopping power for 400 AMeV iron beam and 20 g/cm^2 upstream polyethylene target thickness. (b) Proton stopping power graph for a graphite target [40].

References

[1] R. S. Balmer, J. R. Brandon, S. L. Clewes et al., "Chemical vapour deposition synthetic diamond: materials, technology and applications," *Journal of Physics: Condensed Matter*, vol. 21, no. 36, p. 364221, 2009.

[2] H. El-Hajj, A. Denisenko, A. Bergmaier, G. Dollinger, M. Kubovic, and E. Kohn, "Characteristics of boron δ-doped diamond for electronic applications," *Diamond and Related Materials*, vol. 17, no. 4–5, pp. 409–414, 2008.

[3] R. S. Sussmann, *CVD Diamond for Electronic Devices and Sensors*, John Wiley & Sons, West Sussex, UK, 2009.

[4] P. Forsberg and M. Karlsson, "High aspect ratio optical gratings in diamond," *Diamond and Related Materials*, vol. 34, pp. 19–24, 2013.

[5] J. Isberg, "High carrier mobility in single-crystal plasma-deposited diamond," *Science*, vol. 297, no. 5587, pp. 1670–1672, 2002.

[6] J. Isberg, J. Hammersberg, H. Bernhoff, D. J. Twitchen, and A. J. Whitehead, "Charge collection distance measurements in single and polycrystalline CVD diamond," *Diamond and Related Materials*, vol. 13, no. 4–8, pp. 872–875, 2004.

[7] M. Artuso, F. Bachmair, L. Bani et al., "A 3D diamond detector for particle tracking," *Nuclear Instruments and Methods in Physics Research Section A: Accelerators, Spectrometers, Detectors and Associated Equipment*, vol. 824, pp. 402–405, 2016.

[8] S. Lagomarsino, M. Bellini, C. Corsi et al., "Pulsed laser fabrication of 3D diamond detectors," in *Proceedings of RD13–11th International Conference on Large Scale Applications and Radiation Hardness of Semiconductor Detectors*, Florence, Italy, July 2013.

[9] M. Pillon, M. Angelone, G. Aielli et al., "Radiation tolerance of a high quality synthetic single crystal chemical vapor deposition diamond detector irradiated by 14.8 MeV neutrons," *Journal of Applied Physics*, vol. 104, no. 5, p. 054513, 2008.

[10] A. Metcalfe, G. R. Fern, P. R. Hobson, D. R. Smith, G. Lefeuvre, and R. Saenger, "Diamond based detectors for high temperature, high radiation environments," *Journal of Instrumentation*, vol. 12, no. 1, p. C01066, 2017.

[11] E. Lukosi, "Microfluidic alpha spectrometry of UOX PWR UNF in a molten salt," *Nuclear Science and Engineering*, vol. 188, no. 3, pp. 294–302, 2017.

[12] M. Angelone, M. Pillon, G. Prestopino et al., "Thermal and fast neutron dosimetry using artificial single crystal diamond detectors," *Radiation Measurements*, vol. 46, no. 12, pp. 1686–1689, 2011.

[13] J. A. Davis, K. Ganesan, D. A. Prokopovich et al., "A 3D lateral electrode structure for diamond based microdosimetry," *Applied Physics Letters*, vol. 110, no. 1, p. 013503, 2017.

[14] R. Pilotti, M. Angelone, M. Marinelli et al., "High-temperature long-lasting stability assessment of a single-crystal diamond detector under high-flux neutron irradiation," *EPL*, vol. 116, no. 4, p. 42001, 2016.

[15] S. Almaviva, M. Angelone, M. Marinelli et al., "Characterization of damage induced by heavy neutron irradiation on multilayered ^{6}LiF-single crystal chemical vapor deposition diamond detectors," *Journal of Applied Physics*, vol. 106, no. 7, p. 073501, 2009.

[16] M. Rebai, A. Milocco, L. Giacomelli et al., "Response of a single-crystal diamond detector to fast neutrons," *Journal of Instrumentation*, vol. 8, no. 10, p. P10007, 2013.

[17] E. Lukosi, J. Littell, H. Hale et al., "First design of a diamond-based neutron spectrometer for cross section measurements," in *Nuclear Science Symposium and Medical Imaging Conference (NSS/MIC)*, Seoul, Korea, October 2013.

[18] E. Lukosi, M. Prelas, and J. Palsmeier, "Monte Carlo simulations of multiplexed electronic grade CVD diamond for neutron detection," *Radiation Measurements*, vol. 47, no. 6, pp. 417–425, 2012.

[19] V. N. Amosov, S. A. Meshaninov, N. B. Rodionov, and R. N. Rodionov, "Fast neutron diamond spectrometer," *Diamond and Related Materials*, vol. 20, pp. 1239–1242, 2011.

[20] A. Lohstroh, P. J. Sellin, S. Gkoumas et al., "The effect of fast neutron irradiation on the performance of synthetic single crystal diamond particle detectors," *Diamond and Related Materials*, vol. 19, no. 7–9, pp. 841–845, 2010.

[21] D. Lattanzi, M. Angelone, M. Pillon et al., "Single crystal CVD diamonds as neutron detectors at JET," *Fusion Engineering and Design*, vol. 84, no. 7–11, pp. 1156–1159, 2009.

[22] M. Pillon, M. Angelone, D. Lattanzi et al., "Neutron detection at jet using artificial diamond detectors," *Fusion Engineering and Design*, vol. 82, no. 5–14, pp. 1174–1178, 2007.

[23] J. W. Tsung, M. Havranek, F. Hügging, H. Kagan, H. Krüger, and N. Wermes, "Signal and noise of diamond pixel detectors at high radiation fluences," *Journal of Instrumentation*, vol. 7, no. 9, p. P09009, 2012.

[24] V. Grilj, M. Jakšić, N. Skukan et al., "Irradiation of thin diamond detectors and radiation hardness tests using MeV protons," *Nuclear Instruments and Methods in Physics Research Section B: Beam Interactions with Materials and Atoms*, vol. 306, pp. 191–194, 2013.

[25] I. Zamboni, Ž. Pastuović, and M. Jakšić, "Radiation hardness of single crystal CVD diamond detector tested with MeV energy ions," *Diamond and Related Materials*, vol. 31, pp. 65–71, 2013.

[26] A. Oh, "Development and test of a 3D diamond detector for ionising radiation," in *Proceedings of IEEE NSS/MIC/RSTD*, Seoul, Korea, July 2013.

[27] S. Michimasa, M. Takaki, M. Dozono et al., "Development of CVD diamond detector for time-of-flight measurements," *Nuclear Instruments and Methods in Physics Research Section B: Beam Interactions with Materials and Atoms*, vol. 317, pp. 710–713, 2013.

[28] M. Pomorski, E. Berdermann, A. Caragheorgheopol et al., "Development of single-crystal CVD-diamond detectors for spectroscopy and timing," *Physica Status Solidi (A)*, vol. 203, no. 12, pp. 3152–3160, 2006.

[29] M. Rebai, C. Cazzaniga, G. Croci et al., "Pixelated single-crystal diamond detector for fast neutron measurements," *Journal of Instrumentation*, vol. 10, no. 3, p. C03016, 2015.

[30] W. Adam, W. De Boer, E. Borchi et al., "Radiation hard diamond sensors for future tracking applications," *Nuclear Instruments and Methods in Physics Research Section A: Accelerators, Spectrometers, Detectors and Associated Equipment*, vol. 565, no. 1, pp. 278–283, 2006.

[31] C. Alpigiani, N. Venturi, J. Saxon, S. Valenitinetti, A. Schorlemmer, and A. Gorisek, "ATLAS tracking, beam protection and forward detector systems," No. ATL-INDET-SLIDE-2013-144, ATL-COM-INDET-2013-009, 2013.

[32] W. De Boer, J. Bol, A. Furgeri et al., "Radiation hardness of diamond and silicon sensors compared," *Physica Status Solidi (A)*, vol. 204, no. 9, pp. 3004–3010, 2007.

[33] A. Gobbi, J. P. Alard, G. Augustinski et al., "A highly-segmented ΔE-time-of-flight wall as forward detector of the 4π-system for charged particles at the SIS/ESR accelerator," *Nuclear Instruments and Methods in Physics Research Section A: Accelerators, Spectrometers, Detectors and Associated Equipment*, vol. 324, no. 1-2, pp. 156–176, 1993.

[34] M. Shao, O. Barannikova, X. Dong et al., "Extensive particle identification with TPC and TOF at the STAR experiment," *Nuclear Instruments and Methods in Physics Research Section A: Accelerators, Spectrometers, Detectors and Associated Equipment*, vol. 558, no. 2, pp. 419–429, 2006.

[35] S. Agostinelli, J. Allison, K. Amako, and G. Barrand, "GEANT4—a simulation toolkit," *Nuclear Instruments and Methods in Physics Research Section A: Accelerators, Spectrometers, Detectors and Associated Equipment*, vol. 506, no. 3, pp. 250–303, 2003.

[36] R. Fox, C. Bolen, K. Orji et al., "NSCLSpecTcl meeting the needs of preliminary nuclear physics data analysis," in *Proceedings of 11th Annual Tcl/Tk Conference*, New Orleans, LA, USA, February 2004.

[37] A. Heikkinen, *Implementing the Bertini Intra-Nuclear-Cascade in the Geant4 Hadronic Framework*, American Nuclear Society Monte Carlo Topical Meeting, Chattanooga, TN, USA, 2005.

[38] N. A. McGirl, L. A. Castellanos, A. P. Srikrishna et al., "Accelerator-based measurements relevant for shielding design in space," in *Proceedings of Aerospace Conference*, Big Sky, MT, USA, March 2016.

[39] H. Bethe and W. Heitler, *On the Stopping of Fast Particles and on the Creation of Positive Electrons*, The Royal Society, London, UK, 1934.

[40] M. J. Berger, *ESTAR, PSTAR and ASTAR: Computer Programs for Calculating Stopping Powers and Ranges for Electrons, Protons and Helium Ions*, National Bureau of Standards, Gaithersburg, MA, USA, 1995.

[41] Z. Ge, Z. X. Zhao, H. H. Xia et al., "The updated version of Chinese evaluated nuclear data library (CENDL-3.1)," *Journal of the Korean Physical Society*, vol. 59, no. 2, pp. 1052–1056, 2011.

[42] D. Griffiths, *Introduction to Elementary Particles*, John Wiley & Sons, Hoboken, NJ, USA, 2008.